

From Gapped Excitons to Gapless Triplons in One Dimension

M. Hafez Torbati,^{1,*} Nils A. Drescher,^{1,†} and Götz S. Uhrig^{1,‡}

¹*Lehrstuhl für Theoretische Physik I, Technische Universität Dortmund,
Otto-Hahn-Straße 4, 44221 Dortmund, Germany*

(Dated: October 8, 2018)

Often, exotic phases appear in the phase diagrams between conventional phases. Their elementary excitations are of particular interest. Here, we consider the example of the ionic Hubbard model in one dimension. This model is a band insulator (BI) for weak interaction and a Mott insulator (MI) for strong interaction. Inbetween, a spontaneously dimerized insulator (SDI) occurs which is governed by energetically low-lying charge and spin degrees of freedom. Applying a systematically controlled version of the continuous unitary transformations (CUTs) we are able to determine the dispersions of the elementary charge and spin excitations and of their most relevant bound states on equal footing. The key idea is to start from an externally dimerized system using the relative weak interdimer coupling as small expansion parameter which finally is set to unity to recover the original model.

PACS numbers: 71.30.+h,71.10.Li,71.10.Fd

I. INTRODUCTION

In condensed matter physics, an important focus is the understanding of the phases which determine the qualitative behavior of the systems under study. In strongly correlated systems, in particular, a large variety of phases may occur. In order to understand their physical properties their static and dynamic correlations have to be described. We focus here on the dynamic correlations of strongly interacting electronic systems which display insulating behavior in certain parameter regimes. Our key issue is to understand and to describe the elementary excitations, also called quasiparticles, and possible bound states formed by them.

At commensurate fillings of electronic bands the band insulator (BI) and the Mott insulator (MI) represent two distinct classes of insulating systems which exhibit distinct excitations. In a BI, the spin and charge gaps are both finite and equal. These finite gaps in the charge and in the spin channel originate from the electron-ion interactions¹. The interaction among the electrons may be arbitrarily weak. The elementary excitations in a BI are electrons or holes. A pair of an electron and a hole may form non-magnetic singlet and/or magnetic triplet bound state(s) due to the attractive two-particle interaction.

A MI is characterized by spin and charge excitations which display different dispersions. The MI phase is stabilized by a strong electron-electron interaction^{1,2}. There is no MI without sufficiently strong interaction between the charges. In the MI, single charges (electron or hole quasiparticles) are gapped with a significant gap of the order of the interaction. For large repulsive interactions, the magnetic excitations are described by Heisenberg models with antiferromagnetic exchange. The precise properties of the magnetic excitations strongly depend on further details of the underlying lattice. Both gapped and gapless magnetic excitations may occur.

In one dimension, the elementary spin excitations in

MI are established to be spinons which carry the total spin $S = 1/2$ and show a gapless linear dispersion at the edge of the Brillouin zone (BZ)^{3,4}. For any infinitesimal dimerization confinement occurs: Bound states of two spinon with total spin $S = 1$, called triplon, occur and constitute the elementary excitations⁵⁻¹⁰. In higher dimensions, the conventional scenario is the occurrence of phases with long range magnetic order. The generic excitations are magnons, i.e., gapless Goldstone bosons with integer spin¹¹. But in case of strongly competing interactions, for instance if three spins should align mutually antiparallel to satisfy their interactions, far more complex behavior may occur. In particular in two dimensions, gapped excitations with anyonic statistics may occur¹².

A general motif for exotic phases to occur are competing driving forces: If there is a control parameter of the system which implies that the system is in the conventional phase A in one limit and in phase B in the other, it is promising to look closely what happens at the transition from A to B. Often, a third phase C occurs in which the main driving forces essentially cancel, leaving room for novel ordering mechanisms. Following this spirit, we study the competition of two driving forces acting directly on the charges. The two competing, rather conventional phases are the BI and the MI. The control parameter is the ratio between an on-site repulsion U and an alternating local potential δ .

The simplest model with these antagonists is the ionic Hubbard model (IHM). The model consists of the usual Hubbard model plus a staggered ionic potential δ which splits the energy on even and odd sites. Its Hamiltonian in 1D is given by

$$H = \frac{\delta}{2} \sum_{i,\sigma} (-1)^i n_{i,\sigma} + U \sum_i \left(n_{i,\uparrow} - \frac{1}{2} \right) \left(n_{i,\downarrow} - \frac{1}{2} \right) + t \sum_{i,\sigma} \left(c_{i,\sigma}^\dagger c_{i+1,\sigma} + \text{H.c.} \right), \quad (1)$$

where the operators $c_{i,\sigma}^\dagger$ and $c_{i,\sigma}$ are the fermionic oper-

ators creating and annihilating an electron with spin σ at site i . The operator $n_{i,\sigma} := c_{i,\sigma}^\dagger c_{i,\sigma}$ counts the number of spin- σ electrons at site i .

Clearly, the MI phase is stable if the Hubbard interaction is the dominant term in the system while the BI becomes the ground state if the ionic potential prevails over the other model parameters. It is shown that the MI and the BI are separated by an intermediate phase in 1D which is known to be a spontaneously dimerized insulator (SDI)^{13–18}. In two dimensions, however, the nature of the middle phase is highly disputed^{19–23}.

The IHM was first proposed^{24–26} to describe the neutral-ionic transition in the charge-transfer mixed-stack organic compounds like TTF-chloranil²⁷. Later, it was shown that the model is also a candidate to explain the ferroelectricity in transition metal oxides such as BaTiO₃²⁸. Transition metal oxides and mixed-stack organic compounds²⁹ are both interesting classes of solids which supports the relevance of the IHM beyond its theoretical significance.

In the present article, we explore the excitation spectrum of the one-dimensional IHM at zero temperature and half-filling using *directly evaluated enhanced perturbative continuous unitary transformations* (deepCUT)³⁰. The underlying idea is to map the microscopic Hamiltonian (1) to an effective model expressed directly in the elementary excitations. This mapping is systematically controlled by some small parameter. In previous work, we started from the BI in which the elementary excitations are unbound, but dressed fermions: Quasiparticles and quasiholes^{18,31,32}. The resulting effective model can be used within the BI phase and to some extent in the adjacent SDI phase. But the dispersion in the SDI phase and the MI phase cannot be treated. For this reason, we take a different view point in the present work.

We start from the dimer limit where the system is composed of isolated dimers^{33,34} and turn on the inter-dimer hopping in the renormalization scheme of the deepCUT³⁰. The advantage of the dimer limit, compared to the BI limit¹⁸, is that it allows us to access all the three different phases of the IHM. We look for the transition points U_{c1} between the BI and the SDI phase and U_{c2} between the SDI and the MI phase by analyzing the ground state energy and various energy gaps. The results are compared to data from a density matrix renormalization (DMRG) calculation¹⁷. The main focus, however, will lie on the momentum dependent low-energy spectrum in the three phases: BI, SDI, and MI.

In the BI phase, we verify that the approach from the dimer limit satisfactorily reproduces the deepCUT results obtained from the BI limit¹⁸. In the intermediate SDI phase, both charge and spin degrees of freedom contribute to the low-energy spectrum. We discuss the difficulties of the electron-hole picture to explain this excitation spectrum. In the MI phase, it is found that the low-energy physics of the IHM for large enough Hubbard interaction can be described by an effective Hamiltonian *purely* in terms of magnetic triplon operators in the spirit

of the description of spin chains from the dimer limit in Ref. 9. The analysis of the ensuing effective triplon Hamiltonian yields quantitative results for the gapless triplon dispersion of the IHM in the MI phase.

The article is set up in the following way. After this Introduction, we discuss the dimer limit and its local excitations in detail in Sect. II. Section III is devoted to a brief discussion of technical aspects. Next, we present results for the ground state energy and the gaps to the lowest excitations in Sect. IV. In Sect. V we elucidate the dispersions, i.e., the full momentum dependence of the elementary excitations in the BI, in the SDI, and in the MI phase. Finally, the article is concluded in Sect. VI.

II. DIMER LIMIT

The IHM (1) has a four dimensional Hilbert space at each site: The empty state, the spin up and down states, and the doubly occupied state. However, the empty states on odd sites and the doubly occupied states on even sites lie very high in energy for $U, \delta \gg t$. In the following, we limit our analysis of the IHM to the case where $U, \delta \gg t$ and truncate the Hilbert space such that no empty state on odd sites and no doubly occupied state on even sites is considered. We stress that such a restriction has no qualitative effect on the phase diagram of the IHM for small hopping t .

In addition, a DMRG study shows that the position of the transition points of the IHM with the truncated Hilbert space quite accurately match the results of the IHM considering the full Hilbert space in the limit $U, \delta \gg t$. For instance, $t = \delta/20$, $U_{c1} = 1.065\delta$ in the truncated case¹⁷ and $U_{c1} = 1.069\delta$ in the untruncated case¹⁵. Of course, one could apply a first CUT to eliminate the high energy states as we did in previous work¹⁸. In view of the minute difference in number we refrain from this first step in order to keep the initial Hamiltonian as simple as possible. But we stress that for larger ratios t/δ such a first step is indicated.

We will treat the odd and even sites in the same way by restoring the translational invariance by an electron-hole transformation on the odd sites

$$c_{i,\sigma}^\dagger \rightarrow \eta_\sigma h_{i,\bar{\sigma}}, \quad (2)$$

where $\eta_\uparrow = 1$, $\eta_\downarrow = -1$, and $\bar{\sigma}$ stands for the opposite direction of the spin. Unifying the electron and hole operators by the fermion operator

$$f_{i,\sigma} := \begin{cases} c_{i,\sigma} & \text{for } i \in \text{even,} \\ h_{i,\sigma} & \text{for } i \in \text{odd,} \end{cases} \quad (3)$$

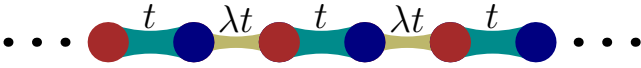


Figure 1. (Color online) Schematic representation of dimer limit expansion. The intradimer hopping parameter is denoted by t , the interdimer hopping by λt . For $\lambda = 0$ the system consists of isolated dimers and for $\lambda = 1$ the uniform chain is retrieved.

maps the Hamiltonian (1) to the form

$$H = \frac{U-2\delta}{4} \sum_i \mathbb{1} + t \sum_{i,\sigma} \eta_\sigma (f_{i,\sigma}^\dagger f_{i+1,\bar{\sigma}} + \text{H.c.}) + \frac{\delta-U}{2} \sum_{i,\sigma} f_{i,\sigma}^\dagger f_{i,\sigma} + U \sum_i f_{i,\uparrow}^\dagger f_{i,\downarrow}^\dagger f_{i,\downarrow} f_{i,\uparrow}. \quad (4)$$

In this operator representation, omitting all the doubly occupied states is equivalent to omitting the empty states on the odd sites and the doubly occupied states on the even sites in the original picture (1) as we intended to do.

Hubbard operators are used to decompose the Hamiltonian (4) into the terms which create or annihilate specific numbers of double occupancies. The Hubbard operators are defined by

$$g_{i,\sigma}^\dagger := |\sigma\rangle_i \langle e|, \quad (5a)$$

$$g_{i,d}^\dagger := |d\rangle_i \langle e|, \quad (5b)$$

where $\sigma = \uparrow, \downarrow$ stands for the spin direction while d and e stand for the doubly occupied state and the empty state, respectively. The f -operator in terms of Hubbard operators is given by

$$f_{i,\sigma}^\dagger = g_{i,\sigma}^\dagger + \eta_\sigma g_{i,d}^\dagger g_{i,\bar{\sigma}}. \quad (6)$$

Finally, inserting Eq. (6) and its hermitian conjugate into the Hamiltonian (4) and only keeping the terms which matter for the subspace with zero double occupancies yields

$$H = \frac{U-2\delta}{4} \sum_i \mathbb{1} + \frac{\delta-U}{2} \sum_{i,\sigma} g_{i,\sigma}^\dagger g_{i,\sigma} + t \sum_{i,\sigma} \eta_\sigma (g_{i,\sigma}^\dagger g_{i+1,\bar{\sigma}} + \text{H.c.}). \quad (7)$$

In order to use the dimer limit, see Fig. 1, as starting point for the intended deepCUT analysis we modify the Hamiltonian (7) such that it takes the form

$$H = \frac{U-2\delta}{4} \sum_i \mathbb{1} + \frac{\delta-U}{2} \sum_{i,\sigma} g_{i,\sigma}^\dagger g_{i,\sigma} + t \sum_{i \in \text{even}, \sigma} \eta_\sigma (g_{i,\sigma}^\dagger g_{i+1,\bar{\sigma}} + \lambda g_{i+1,\sigma}^\dagger g_{i+2,\bar{\sigma}} + \text{H.c.}), \quad (8)$$

where λ is the perturbative parameter on which we base the truncation of the flow equations in the deepCUT³⁰.

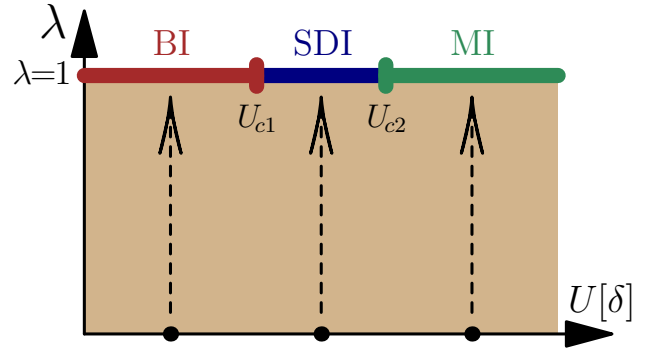


Figure 2. (Color online) Schematic phase diagram of the model (8) for a fixed value of the hopping parameter. The system is dimerized for all values $\lambda < 1$. At $\lambda = 1$ we reach the phase diagram of the ionic Hubbard model (IHM). By choosing an appropriate value for the Hubbard interaction U and increasing the parameter λ from 0 to 1 we can describe different phases of the IHM: the band insulator (BI), the spontaneously dimerized insulator (SDI), and the Mott insulator (MI).

For $\lambda = 0$ the Hamiltonian is composed of isolated dimers and for $\lambda = 1$ the uniform IHM (7) is retrieved. By fixing an appropriate value for the Hubbard interaction U and increasing the parameter λ from 0 to 1 we access the three different phases of the IHM, see Fig. 2. One notices that the BI and the MI phases are both on the border of the phase diagram.

For applying the deepCUT method, we re-express the Hamiltonian (8) in terms of creation and annihilation operators of the elementary excitations on a dimer. For vanishing interdimer hopping, $\lambda = 0$, the system consists of independent dimers with a nine dimensional local Hilbert space. The nine eigenstates and eigenvalues of a single dimer are summarized in Table I. The ground state energy ϵ_0 , the triplon energy ϵ_t , the fermion energy ϵ_f , and the singlon energy ϵ_s are found to be

$$\epsilon_0 = -\frac{1}{2} \left(\delta + \sqrt{(U-\delta)^2 + 8t^2} \right), \quad (9a)$$

$$\epsilon_t = +\frac{1}{2} \left(\delta - U + \sqrt{(U-\delta)^2 + 8t^2} \right), \quad (9b)$$

$$\epsilon_s = 2\epsilon_f = \sqrt{(U-\delta)^2 + 8t^2}. \quad (9c)$$

The coefficients α and β are given by

$$\alpha = \sqrt{\frac{1}{2} + \frac{U-\delta}{4\epsilon_f}}, \quad (10a)$$

$$\beta = \sqrt{\frac{1}{2} - \frac{U-\delta}{4\epsilon_f}}. \quad (10b)$$

For all values of the parameters t , U , and δ , the state with lowest energy has total spin zero and it is denoted as vacuum $|0\rangle$. There are four degenerate fermionic excited states corresponding to the fermion being placed on the

Table I. Eigenstates and eigenvalues of a single dimer of Hamiltonian (8), i.e., at $\lambda = 0$. There are three different possible states on each site: empty state e , spin up state \uparrow , and spin down \downarrow state. This leads to nine eigenstates on each dimer. The ground state has total spin zero and is denoted as vacuum by $|0\rangle$. There are four fermionic and four bosonic excited states. The expressions ϵ_0 , ϵ_t , ϵ_f , and ϵ_s are defined in Eq. (9) and the coefficients α and β are given in Eq. (10).

#	Dimer Eigenstates	Eigenvalues
1	$ 0\rangle = -\beta e, e\rangle + \frac{\alpha}{\sqrt{2}}(\uparrow, \downarrow\rangle - \downarrow, \uparrow\rangle)$	ϵ_0
2	$ t\rangle_{+1} = \uparrow, \uparrow\rangle$	$\epsilon_0 + \epsilon_t$
3	$ t\rangle_0 = \frac{1}{\sqrt{2}}(\uparrow, \downarrow\rangle + \downarrow, \uparrow\rangle)$	$\epsilon_0 + \epsilon_t$
4	$ t\rangle_{-1} = \downarrow, \downarrow\rangle$	$\epsilon_0 + \epsilon_t$
5	$ f\rangle_{l,\uparrow} = \uparrow, e\rangle$	$\epsilon_0 + \epsilon_f$
6	$ f\rangle_{l,\downarrow} = \downarrow, e\rangle$	$\epsilon_0 + \epsilon_f$
7	$ f\rangle_{r,\uparrow} = e, \uparrow\rangle$	$\epsilon_0 + \epsilon_f$
8	$ f\rangle_{r,\downarrow} = e, \downarrow\rangle$	$\epsilon_0 + \epsilon_f$
9	$ s\rangle = +\alpha e, e\rangle + \frac{\beta}{\sqrt{2}}(\uparrow, \downarrow\rangle - \downarrow, \uparrow\rangle)$	$\epsilon_0 + \epsilon_s$

left site $|f\rangle_{l,\sigma}$ or on the right site $|f\rangle_{r,\sigma}$ and it may take one of two different spin states $\sigma = \uparrow, \downarrow$.

Among the four bosonic excited states, there is one state with total spin zero $|s\rangle$, which we call singlon hence-

The Hubbard g -operators can be expressed in terms of the dimer excitation operators

$$g_{j;l,\sigma}^\dagger = -\beta f_{j;l,\sigma}^\dagger + t_{j;\eta_\sigma}^\dagger f_{j;r,\sigma} + \alpha f_{j;l,\sigma}^\dagger s_j + \frac{1}{\sqrt{2}} \left(\eta_\sigma \alpha + t_{j;0}^\dagger + \eta_\sigma \beta s_j^\dagger \right) f_{j;r,\bar{\sigma}}, \quad (12a)$$

$$g_{j;r,\sigma}^\dagger = -\beta f_{j;r,\sigma}^\dagger - t_{j;\eta_\sigma}^\dagger f_{j;l,\sigma} + \alpha f_{j;r,\sigma}^\dagger s_j + \frac{1}{\sqrt{2}} \left(\eta_\sigma \alpha - t_{j;0}^\dagger + \eta_\sigma \beta s_j^\dagger \right) f_{j;l,\bar{\sigma}}, \quad (12b)$$

where $g_{j;l,\sigma}^\dagger$ and $g_{j;r,\sigma}^\dagger$ act on the left and on the right site, respectively, of dimer j . Finally, the Hamiltonian (8) in terms of dimer excitation operators reads

$$H = \epsilon_0 \sum_j \mathbb{1} + \sum_j \sum_{m=\pm 1,0} \epsilon_t t_{j;m}^\dagger t_{j;m} + \sum_j \epsilon_s s_j^\dagger s_j + \sum_{j,\sigma} \sum_{p=l,r} \epsilon_f f_{j;p,\sigma}^\dagger f_{j;p,\sigma} + \lambda t \sum_{j,\sigma} \eta_\sigma \left(g_{j;r,\sigma}^\dagger g_{j+1;l,\bar{\sigma}}^\dagger + \text{H.c.} \right), \quad (13)$$

where the sum j runs over the dimer positions instead of the original sites. In the last term, the Hubbard g -operators is meant to be replaced according to Eq. (12). We do not display the resulting expression explicitly for the sake of brevity.

If no interdimer hopping is included, the dimer excitations are the true quasiparticles of the system. But for any finite value of the relative interdimer hopping λ the dimer excitations start to propagate in the lattice and become dressed quasiparticles. To remind the reader of this dressing, we refer to them as singlon and triplon and not as singlet and triplet. In the next Sects. IV and V, the Hamiltonian (13) is mapped continuously to effective Hamiltonians such that the dimer excitations can still be used as quasiparticles of the system even for $\lambda \neq 0$.

forth, and a three-fold degenerate triplet with total spin one and magnetic quantum numbers $|t\rangle_{\pm 1,0}$, which we call triplon henceforth. It is seen from Eqs. (9b) and (9c) that the local singlon energy ϵ_s is twice the fermion energy ϵ_f . The triplon energy ϵ_t and the fermion energy ϵ_f are close to each other for $U \approx \delta$. This makes it difficult to decouple the two-fermion sector, the two-triplon sector, and the one-singlon sector from one another in the deepCUT.

Next, we define the following local hardcore creation operators at the *dimer* position j

$$f_{j;p,\sigma}^\dagger := |f\rangle_{j;p,\sigma} \langle 0| \quad ; \quad p = l, r \quad (11a)$$

$$t_{j;m}^\dagger := |t\rangle_{j;m} \langle 0| \quad ; \quad m = \pm 1, 0 \quad (11b)$$

$$s_j^\dagger := |s\rangle_j \langle 0|. \quad (11c)$$

The fermion operator $f_{j;p,\sigma}^\dagger$ creates a fermionic excitation from the vacuum at dimer j with spin σ at the internal position $p = l$ or r where l stands for the left position and r for the right one. Similarly, the triplon operator $t_{j;m}^\dagger$ and the singlon operator s_j^\dagger create a triplon with magnetic number m and a singlon at the dimer position j , respectively. Summarizing, we call these operators of second quantization ‘‘dimer excitation operators’’.

III. SOME TECHNICAL ASPECTS

Continuous unitary transformations (CUTs) or the flow equation method^{35,36} represents the basis of various perturbative^{7,37,38} and renormalization approaches^{30,39–41}. The basic flow equation reads

$$\partial_\ell H(\ell) = [\eta(\ell), H(\ell)] \quad (14)$$

where ℓ is an auxiliary parameter which parametrizes the unitary transformation and changes from $\ell = 0$ to $\ell = \infty$. The important choice is how the Hamiltonian is transformed which amounts up to the choice of the infinitesimal generator $\eta(\ell) = -\eta(\ell)^\dagger$. Once one has chosen

a basis for operators in order to be able to write general operators as linear combinations, the differential equation (14) induces differential equations in the coefficients for the basis operators. Generally, the required number of basis operators is infinite.

The deepCUT is a renormalizing approach which truncates the contributions to these differential equations on the basis of their order in the expansion parameter. The idea is to *target* a certain quantity, for instance the ground state energy and perhaps the dispersions, in a certain order n . Then all contributions in the flow equations which are relevant for the targeted quantities up to order n are kept, but contributions which matter only in higher orders are neglected. Finally, the resulting set of differential equations is solved numerically. Thereby, the data obtained comprises contributions in all orders in the expansion parameter, but it is still approximate.

Increasing the targeted order we study whether the results still change significantly. If the results do not depend on the order of the calculations they can be considered reliable. For further technical aspects of the deepCUT approach we refer the reader to Ref. 30.

Here we discuss specific aspects of the generator that we employ. The general aim is to obtain an effective Hamiltonian which conserves the number of excitations^{7,42}. To this end, a particle-conserving generator is used which consists of the terms occurring in the Hamiltonian with a relative sign depending on the change of the number of quasiparticles: Positive for terms incrementing this number and negative for terms decreasing it.

Because the unperturbed part of the Hamiltonian (13) has a non-equidistant spectrum, the mere number of excitations is not a suitable criterion to decide about the sign in the generator. We use the sign of the change in the local energy instead. Assume $H_{a_t, a_f, a_s}^{c_t, c_f, c_s}$ stands for the part of the Hamiltonian which creates c_t triplons, c_f fermions, and c_s singlons and annihilates a_t triplons, a_f fermions, and a_s singlons. Then this part contributes to the generator according to

$$\hat{\eta} [H_{a_t, a_f, a_s}^{c_t, c_f, c_s}(\ell)] = \text{sign}(\Delta\epsilon(\ell)) H_{a_t, a_f, a_s}^{c_t, c_f, c_s}(\ell), \quad (15)$$

where the local energy change $\Delta\epsilon(\ell)$ is defined by

$$\Delta\epsilon(\ell) := (c_t - a_t)\epsilon_t(\ell) + (c_f - a_f)\epsilon_f(\ell) + (c_s - a_s)\epsilon_s(\ell). \quad (16)$$

The functions $\epsilon_t(\ell)$, $\epsilon_f(\ell)$, and $\epsilon_s(\ell)$ are the onsite energies of triplons, fermions, and singlons in the course of the flow ℓ . Their initial values at $\ell = 0$ are given in Eq. (9).

In order to set up the differential equations in high targeted order n certain simplification rules are used. Their key idea is to identify unnecessary contributions early in the calculations to reduce the required memory resources and to avoid cumbersome follow-up computations altogether. The simplification rules that we used in the dimer limit analysis are explained in Appendix A.

IV. GROUND STATE ENERGY AND ENERGY GAPS

A. Ground State Energy

To determine the ground state energy, the state without any singlon, fermion, or triplon has to be decoupled from the remaining Hilbert space. We generalize the definition of the reduced generator introduced in Ref. 42 to the case where there are different kinds of excitations. The ground state generator $\eta_{t;0;f;0;s;0}$ is given by

$$\eta_{t;0;f;0;s;0}(\ell) = \sum_{ijk} \left(\hat{\eta} \left[H_{0,0,0}^{i,j,k}(\ell) \right] - \text{H.c.} \right), \quad (17)$$

where the superoperator $\hat{\eta}$ is defined in Eq. (15). The generator (17) is used to decouple the state with zero number of triplons, fermions, and singlons from subspaces with finite numbers of excitations. We have been able to reach order 12 in the relative interdimer hopping λ targeting the ground state energy (GSE) based on the dimer limit. Finally, all data is shown for $\lambda = 1$.

One may ask what is the maximum range of processes which is captured by targeting the ground state at order 12? To create a pair of fermions with a distance of n dimers we need at least n orders, see Eq. (12). These two fermions can not be canceled individually. We need n additional orders to bring these two fermions to nearest-neighbor (n.n.) dimers and to cancel them. It can be easily seen from Eq. (12) that dealing with bosons (singlon and triplons) is even more costly. Hence, all the terms with an extension larger than $n/2$ are irrelevant at order n targeting the ground state. This is a nice example how one can use simplification rules to avoid unnecessary terms. Therefore, targeting the ground state up to order 12 involves processes with an extension of at most 6 dimers. Since the dimer-dimer distance takes two lattice spacings this corresponds to 12 lattice spacings or more precisely to an extension of 13 lattice spacings since 7 dimers/14 sites are affected by the term.

For comparison, we also analyzed the restricted IHM (7) in the BI limit as we did in Ref. 18 for the IHM with the full Hilbert space, i.e., allowing also for empty states on odd sites and double occupancies on even sites. We stress again that the quantitative differences are very small in the parameter regime considered. Starting from the BI limit, the GSE of the restricted IHM is obtained from a deepCUT up to order 20 in the hopping parameter t . This means that processes up to a range of 10 lattice spacings are included.

The left panel of Fig. 3 depicts the GSE per site extrapolated to infinite order versus the Hubbard interaction U/δ for $t = 0.05\delta$. The right panel of Fig. 3 shows the extrapolation as a linear fit in the inverse order. In the right panel, the parameters are $t = 0.05\delta$ and $U = 1.06\delta, 1.07\delta, 1.08\delta, 1.09\delta, \text{ and } 1.10\delta$ from top to bottom for both the dimer limit (solid circles) and the BI limit (asterisks). The dimer limit results exhibit a faster convergence com-

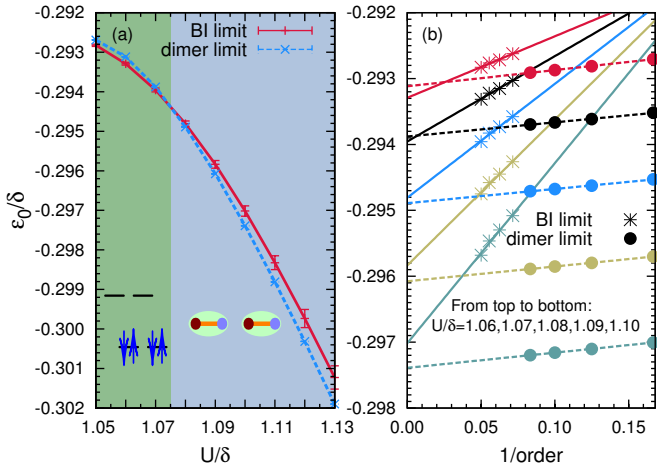


Figure 3. (Color online) Ground state energy per site ϵ_0 of the restricted IHM (7) for $t = 0.05\delta$. The results obtained from both the dimer limit and the BI limit are displayed. In the left panel (a) ϵ_0 extrapolated to infinite order is plotted versus the Hubbard interaction U/δ . Beyond the critical point $U_{c1} = 1.075\delta$, the deepCUT based on the dimer limit yields a lower ground state energy than the calculation based on the BI limit. In the right panel (b), ϵ_0 is depicted versus the inverse order for various values of U . The finite order results are extrapolated linearly to infinite order.

pared to the results from the BI limit. It is seen in Fig. 3 that the GSE obtained from the dimer limit takes lower values than the results from the BI limit beyond the critical Hubbard interaction $U_{c1} = 1.075\delta$ while it is the other way round for lower U . In a rigorous calculation, both results for the GSE have to coincide perfectly in the BI phase. But due to the truncations, the calculation based on the BI limit works better in the BI phase and the one based on the dimer limit works better in the SDI phase. Hence we interpret the results in Fig. 3 as strong evidence for the phase transition BI \rightarrow SDI at the intersection U_{c1} of both curves. For comparison, we state that a DMRG study finds the first transition point of the restricted IHM (7) at $U = 1.065\delta$ ¹⁷ so we conclude that our results are exact within about 1%.

B. Gaps to Excited States

Three different gaps can be defined to measure the energy difference between the ground state and different excited states. The charge gap Δ_c is defined as the energy needed to add an electron to the system plus the energy to take an electron out. It is given by

$$\Delta_c := E_0(N+1) + E_0(N-1) - 2E_0(N), \quad (18a)$$

where $E_0(N)$ stands for the ground state energy of the system with N particles. The singlet exciton gap Δ_e and the spin gap Δ_s are defined as the excitation energy in the channel with the same particle number as the

ground state, but with total spin zero and one, respectively. They read

$$\Delta_e := E_1(N, S=0) - E_0(N, S=0), \quad (18b)$$

$$\Delta_s := E_1(N, S=1) - E_0(N, S=0), \quad (18c)$$

where $E_1(N, S)$ denotes the first excited state with N particle and total spin S . Because we focus on half-filling, we put $N = L$ where L is the lattice size.

In our formalism, the charge gap Δ_c can be accessed by decoupling the ground state and the one-fermion sector (or more sectors) from the other quasiparticle sectors. Once the hopping in the one-fermion sector is known a Fourier transform provides the fermionic dispersion. Twice the minimal energy of this dispersion yields Δ_c . The one-fermion generator $\eta_{t;0;f;1;s;0}$, which separates the ground state and the 1-fermion sector from the remaining Hilbert space, is given by

$$\eta_{t;0;f;1;s;0}(\ell) = \eta_{t;0;f;0;s;0}(\ell) + \eta_{t;0;f;1;s;0}^p(\ell), \quad (19a)$$

where we defined

$$\eta_{t;0;f;1;s;0}^p(\ell) := \sum_{ijk} \left(\hat{\eta} \left[H_{0,1,0}^{i,j,k}(\ell) \right] - \text{H.c.} \right) X_{0,0,0}^{i,j,k}, \quad (19b)$$

with

$$X_{i',j',k'}^{i,j,k} := 1 - \delta_{i,i'} \delta_{j,j'} \delta_{k,k'}. \quad (19c)$$

One needs to include the term $X_{0,0,0}^{i,j,k}$ in Eq. (19b) in order to prevent the interaction $H_{0,1,0}^{0,0,0}$ to appear spuriously twice in the generator (19a).

In a similar way, the one-triplon channel can be decoupled using the one-triplon generator

$$\eta_{t;1;f;0;s;0}(\ell) = \eta_{t;0;f;0;s;0}(\ell) + \eta_{t;1;f;0;s;0}^p(\ell), \quad (20a)$$

with the definition

$$\eta_{t;1;f;0;s;0}^p(\ell) = \sum_{ijk} \left(\hat{\eta} \left[H_{1,0,0}^{i,j,k}(\ell) \right] - \text{H.c.} \right) X_{0,0,0}^{i,j,k}. \quad (20b)$$

The application of the generator (20a) yields an effective Hamiltonian whose one-triplon sector is separated from the remaining Hilbert space. Thus it is easily diagonalized by a Fourier transform leading to the triplon dispersion. Subsequently, the triplon gap can be found as the minimum of the triplon dispersion. The triplon gap is an energy gap in the magnetic spin-1 channel. Still, one must be cautious to identify the triplon gap with the spin gap because there may be another $S = 1$ excitation with a lower energy.

In the two-fermion sector, there is also a channel with total spin one and the true spin gap (18c) is the minimum of the lowest spin-1 two-fermion excitation energy and the triplon gap. Of course, one could imagine even more sophisticated possibilities for spin-1 excitations, but these two cases are clearly the most probable ones. Our results show that the triplon gap is always identical or smaller

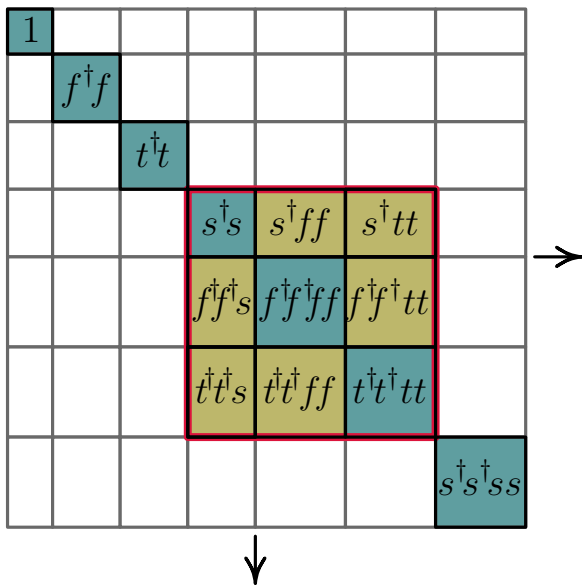


Figure 4. (Color online) General structure of the effective Hamiltonian derived by applying the generator $\eta_{t;2;f;2;s;1}$, defined in Eq. (21), to the initial Hamiltonian (13). The ground state, the one-fermion, and the one-triplon sectors are decoupled from the remainder of the Hilbert space. But the interactions among the one-singlon, the two-fermion, and the two-triplon sector are still present, see red block.

than the spin-1 two-fermion excitation energy and hence we conclude that the triplon gap is indeed the spin gap.

In analogy to the $S = 1$ case, there are also two possibilities for the $S = 0$ gap. Because the singlon quasiparticle has total spin zero, the $S = 0$ gap can be either the singlon gap or the gap in the $S = 0$ two-fermion channel. We find that there is a bound state in the $S = 0$ channel of the two-fermion sector which is significantly lower in energy than the singlon gap. Therefore, the excitation energy of this singlet exciton defines the $S = 0$ gap.

Unfortunately, it is not possible to decouple the two-fermion sector from the other sectors because the local dimer energies of two fermions, two triplons, and one singlon are quite close to one another, see Eqs. (9b) and (9c). Thus, the $S = 0$ gap as well as the low-energy spectrum of the BI phase, see the next section, are calculated using the generator $\eta_{t;2;f;2;s;1}$. This generator decouples the direct sum of the two-fermion sector, the two-triplon sector, and the one-singlon sector from other quasiparticle sectors, see Fig. 4. But the off-diagonal interactions between these three sectors are left out in the generator and thus they persist in the final effective Hamiltonian. Note that they are nevertheless renormalized in the course of the CUT.

The structure of the final effective Hamiltonian is schematically shown in Fig. 4. The generator $\eta_{t;2;f;2;s;1}$

can explicitly be written as

$$\begin{aligned} \eta_{t;2;f;2;s;1}(\ell) &= \eta_{t;0;f;0;s;0}(\ell) + \eta_{t;1;f;0;s;0}^p(\ell) + \eta_{t;0;f;1;s;0}^p(\ell) \\ &+ \sum_{i+j+k \geq 2} \left(\hat{\eta} \left[H_{0,0,1}^{i,j,k}(\ell) \right] - \text{H.c.} \right) X_{2,0,0}^{i,j,k} X_{0,2,0}^{i,j,k} \\ &+ \sum_{i+j+k \geq 2} \left(\hat{\eta} \left[H_{2,0,0}^{i,j,k}(\ell) \right] - \text{H.c.} \right) X_{0,2,0}^{i,j,k} \\ &+ \sum_{i+j+k \geq 2} \left(\hat{\eta} \left[H_{0,2,0}^{i,j,k}(\ell) \right] - \text{H.c.} \right) X_{2,0,0}^{i,j,k}, \quad (21) \end{aligned}$$

where the definitions (19b) and (20b) are used in the first line. It is seen that the off-diagonal interactions $H_{2,0,0}^{0,0,1}$, $H_{0,2,0}^{0,0,1}$, and $H_{0,2,0}^{2,0,0}$ are excluded from the generator (21) using the definition (19c).

The $S = 0$ gap is calculated by an exact diagonalization in the singlet channel of the subspace spanned by the states comprising two fermions, two triplons, or one singlon. The employed exact diagonalization technique is valid in the thermodynamic limit. The only restriction required to deal with a finite-dimensional, numerically tractable problem is the limitation of the distances between two quasiparticles, see Refs. 42 and 18. Since this is a two-particle problem we can treat very large relative distances and find the converged eigenvalues.

Fig. 5 shows various gaps versus the Hubbard interaction U/δ for $t = 0.05\delta$. The results obtained from the BI limit are included for comparison; they are valid only up to the first transition point U_{c1} where the $S = 0$ gap closes. The charge gap Δ_c is calculated up to order 12 in the interdimer hopping from the dimerized limit and up to order 20 in the hopping from the BI limit. Then the finite order results are extrapolated to infinite order by a linear fit to the last four orders as we illustrated for the GSE in the right panel of Fig. 3. From Fig. 5 we see that the charge gap obtained from the dimer limit and from the BI limit agree well up to $U \approx 1.06\delta$ where the charge gap from the dimer limit acquires a minimum. We interpret this minimum as an indication for the first transition point U_{c1} between the BI and the SDI phase^{15,18}.

Next, we discuss the $S = 0$ gap presented in Fig. 5. In the dimer limit approach, order 6 is the maximum order that we can reach for this quantity. Higher orders are not accessible due to divergence in the flow equations. This is induced by overlapping different continua which occurs the more often the more quasiparticles are involved. The same problem occurs for $U > 1.04\delta$. The results of the BI limit in order 12 in the hopping parameter are shown for comparison¹⁸. Again, a divergence of the flow equations prevents us to reach higher orders.

For both limits, the $S = 0$ gap is smaller than the charge gap indicating an $S = 0$ electron-hole bound state, i.e., an exciton, in the BI phase. The $S = 0$ gap obtained from the BI limit at order 12 vanishes at the critical interaction $U_{c1} = 1.067\delta$ which is very close to the DMRG result of the first transition point 1.065δ ¹⁷. The $S = 0$ gap computed from the dimer limit turns out to be too low and in the regime of interest a divergence of the flow

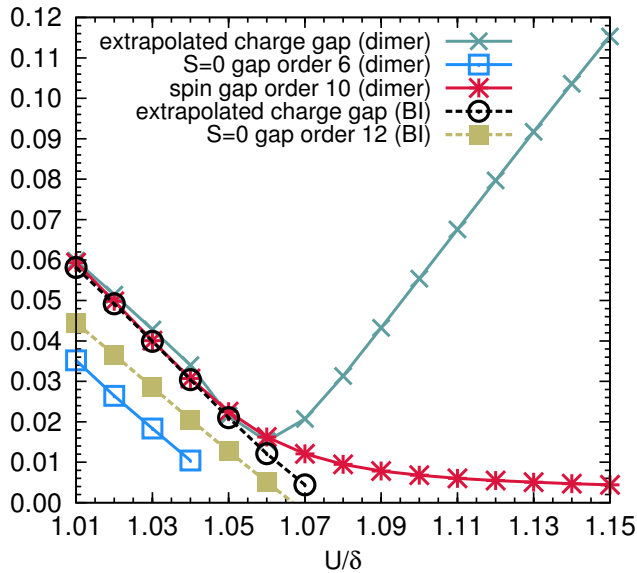


Figure 5. (Color online) The charge gap, the $S = 0$ gap, and the spin (tripion) gap of the Hamiltonian (7) versus the Hubbard interaction U/δ for $t = 0.05\delta$. The results obtained from the BI limit (dashed lines up to $U_{c1} \approx 1.067\delta$, value obtained from the vanishing of the $S = 0$ gap) and the dimer limit (solid lines) are compared.

equation occurs which must be attributed to overlapping continua.

We recall that for the computation of the $S = 0$ bound state we have to separate a large subspace made of up to two excitations from the remaining Hilbert space, see Fig. 4 and for the generator Eq. 21. This aim appears to be too ambitious. We expect that a more sophisticated calculation of the $S = 0$ exciton gap from the dimer limit in finite order will display a non-zero minimum very close to the transition point. Only for extrapolated infinite order this minimum will vanish.

Next, we consider the spin gap (tripion gap) which is obtained up to order 10 in the interdimer hopping parameter λt and plotted versus the interaction U in Fig. 5 for $t = 0.05\delta$. The generator used is the one in Eq. 20a. The results of order 8 almost coincide with the results of order 10 especially inside the BI phase. We did not perform an extrapolation, as we did for the charge gap, because the triplon gap does not display a clear linear behavior versus the inverse order up to order 10. Higher orders would be necessary for an accurate extrapolation to infinite order.

It is seen from Fig. 5 that the spin gap and the charge gaps are very close up to $U = 1.05\delta$. The BI limit analysis shows equal spin and charge gaps up to the transition point $U = 1.067\delta$ within numerical accuracy. We use this fact to estimate the error in the finite order calculations of the spin gap. In fact, the spin gap at the transition point $U = 1.067\delta$ should be about 0.007δ smaller to match the results in the BI limit. If we assume that the spin gap is overestimated by this amount we conclude that

the spin mode becomes soft at $U_{c2} = 1.10\delta$ indicating the second transition from the SDI to the MI. Indeed, this rough estimate is in reasonable agreement with the DMRG result $U_{c2} \simeq 1.085\delta$ ¹⁷.

In finite order, here order 10, the spin gap remains finite even for large values of the Hubbard interaction. This seems to contradict the fact that a second transition to the MI phase occurs at larger interaction^{15,17}. But it must be recalled that the gapless MI phase is unstable versus dimerization, that means, dimerization is a relevant perturbation⁵. Any finite dimerization introduces a finite spin gap in the system. By construction, the deepCUT based on the dimer limit introduces dimerization breaking the symmetry between adjacent bonds, i.e., the reflection symmetry about each site. This broken symmetry is never fully restored in any finite order calculations. Consequently, a finite spin gap remains.

In the next section, we derive a low-energy effective Hamiltonian solely in terms of triplon operators for larger values of the Hubbard interaction, $U \geq 1.15\delta$. This low-energy Hamiltonian is analyzed using a second application of the deepCUT. In this way, we are able to calculate the spin gap up to much higher orders than 10. The extrapolation of the high order results to infinite order clearly show the expected tendency towards zero spin gap in the MI phase.

V. DISPERSIONS

In this section we investigate the momentum dependent low-energy excitation spectrum of the restricted IHM (7) in the BI, in the SDI, and in the MI phase. The momentum dependent excitation spectrum of the IHM in the BI phase has been discussed in Refs. 18, 31, and 32 from the BI limit. Here we will corroborate these findings by results obtained based on the dimer limit. In the SDI and MI phases, the dispersions have not yet been analyzed quantitatively.

A. Band Insulator Phase

In the BI phase, the dressed electrons and holes are the elementary excitations of the system. These fermionic quasiparticles with spin $S = 1/2$ can form singlet or triplet bound states. By starting from the dimer limit, however, we have introduced three different kinds of quasiparticles in the system: Fermions, triplons, and singlons. The latter two are of bosonic character. It is very interesting to see how well the deepCUT calculations based on the dimer limit reproduce the dispersions in the BI phase.

The dispersion of the restricted IHM (7) in the BI phase is obtained by using the generator (21) in the deepCUT. As discussed in the previous section for the $S = 0$ exciton gap, the generator $\eta_{t,2,f,2;s,1}$ maps the initial Hamiltonian (8) to an effective Hamiltonian with the

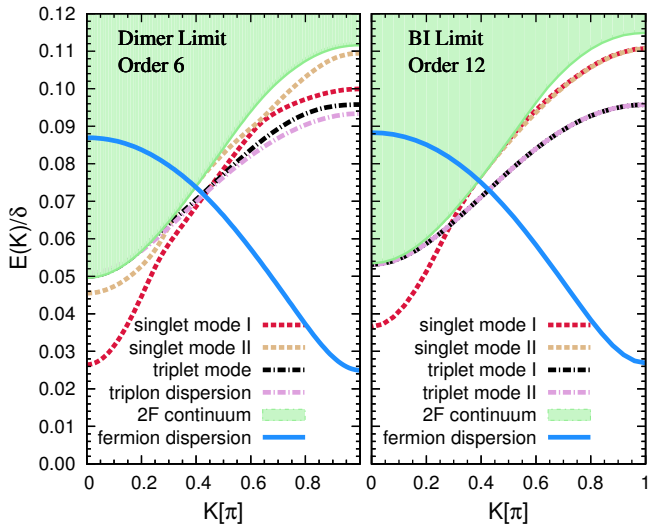


Figure 6. (Color online) The dispersions of Hamiltonian (7) in the BI phase (hopping parameter $t = 0.05\delta$, Hubbard interaction $U = 1.02\delta$). The shaded (colored) area indicates the range of the two-fermion (2F) continuum. The left panel shows the results calculated in the dimer limit analysis in order 6. For comparison, the results from the BI limit in order 12 are plotted in the right panel. Two singlet bound states are found in both the dimer limit and the BI limit calculation. The two triplet modes I and II of the right panel are reproduced in the left panel as a $S = 1$ exciton, called triplet mode, and as a dispersive triplon.

general structure shown in Fig. 4. In this effective Hamiltonian, the one-singlon, two-fermion, and two-triplon sectors are separated as a whole from other sectors. But there are still off-diagonal interactions linking these three sectors among one another.

Because the one-fermion and the one-triplon sectors are decoupled from the rest, the fermion and the triplon dispersions can be obtained by a simple Fourier transformation. The eigenvalues of the Hilbert space composed of the direct sum of the one-singlon, the two-fermion, and the two-triplon subspace are calculated by constructing the Hamiltonian matrix for each specific total momentum, total charge, total spin, and total magnetic number and performing an ED^{18,42}. The employed ED is valid in the thermodynamic limit and we only need to restrict the distances between the quasiparticles^{18,42}. We focus on the sector with no net total charge where the two electrons are of different types. The dimension of the Hamiltonian matrix in the $S = 0$ channel is $3d + 1$ and in the $S = 1$ channel it is $3d$ where d is the maximum distance between quasiparticles. This linear dependence allows us to easily reach very large distances and to find accurate results for the eigenvalues.

The dispersions of the restricted IHM (7) for the parameters $U = 1.02\delta$ and $t = 0.05\delta$ are plotted versus the total momentum K in Fig. 6. In this figure, the lattice spacing between the centers of two dimers, which is twice the distance between two sites, is considered as unit of

length. The left panel of Fig. 6 shows the results obtained from the dimer limit. The BI limit results, which are expected to be more accurate in the BI phase, are depicted in the right panel for comparison.

The BI limit analysis of the IHM is described in Ref. 18 in detail. In Ref. 18 the distance between two *sites* is considered as the unit of length. Thus these results have to be folded to the reduced BZ to compare them with the dimer limit results. The fermion dispersion of the BI limit has also to be shifted by $\pi/2$ on the momentum axis due to a local transformation applied to the fermion operators, see Eq. (16) of Ref. 18.

Orders 6 and 12 are the maximum orders reached in the dimer limit and in the BI limit, respectively. Both analyses involve the same lattice extension because the range of processes taken into account in the deepCUT is proportional to the order of calculations with a factor of 2 for the dimer limit because the lattice distance between two dimers is two lattice spacings.

In the right panel of Fig. 6, there appear two singlet and two triplet bound states in the excitation spectrum obtained from the BI limit. The singlet mode II exists in the momentum range $\pi/2 \lesssim K \leq \pi$ and its energy coincides with the singlet mode I. The two triplet bound states are on top of each other and exist almost in the whole Brillouin zone. The dimer limit also yields two singlet bound states I and II shown in the left panel of Fig. 6. The two singlet modes are not degenerate as in the BI limit because the dimer approach breaks an additional symmetry which is not restored completely due to the truncation of the flow equations. But in view of this approximation the qualitative agreement of the results from both limits is satisfactory. The two degenerate triplet bound states (triplet modes) I and II in the right panel appear also in the left panel with an almost quantitative degeneracy. The agreement of the $S = 1$ results from both limits is very good.

B. Spontaneously Dimerized Phase

The excitation spectrum in the BI phase can be understood well in terms of electrons and holes and their binding phenomena^{18,31}. In the MI phase, the charge degree of freedom appear only at high energies (they are frozen at low energies) and the magnetic low-energy excitations are spinons^{4,43,44} in the uniform case or triplons for any dimerization^{5,9}. The competition between charge and spin degrees of freedom in the 1D IHM leads to an intermediate spontaneously dimerized, insulating phase. In this phase, both charge and spin excitations contribute to the low-energy spectrum of the system making it difficult to determine quantitatively. By construction, the approach based on the dimer limit is especially suited to investigate the SDI phase of the IHM.

We present the results obtained for the fermion dispersion $\omega_f(K)$ (1F in Fig. 7) and the triplon dispersion $\omega_t(K)$ (1T in Fig. 7) in the SDI phase of the IHM. The

fermion dispersion is obtained by the generator (19a) targeting the ground state and the one-fermion sector. Similarly, the triplon dispersion is calculated by the generator (20a) targeting the ground state and the one-triplon sector. The order of the calculations is 12 for the fermion dispersion and 10 for the triplon dispersion in the relative interdimer hopping λ . The two-triplon (2T) continuum, the two-fermion (2F) continuum, and the fermion-triplon (1F1T) continuum are also depicted in Fig. 7. The hopping parameter and the Hubbard interaction are fixed to $t = 0.05\delta$ and $U = 1.08\delta$. The DMRG data¹⁷ indicate that for $t = 0.05\delta$ the SDI phase exists between $U_{c1} = 1.065\delta$ and $U_{c2} \approx 1.085\delta$ so that for $U = 1.080\delta$ we expect the IHM to be in the SDI phase.

The excitation spectrum containing an even number of fermions is plotted in the left panel of Fig. 7. The right panel of Fig. 7 indicates the energy spectrum with an odd number of fermions. The dispersions in Fig. 7 clearly show that *both* the spin and the charge excitations contribute to the low-lying excitation spectrum of the IHM in the SDI. Concomitantly, the two-particle continua play an important role. Thus, we indicate the boundaries of these continua in Fig. 7 as well. The upper band edge of the two-triplon continuum is denoted by $\omega_{2T,+}(K)$ and the lower one by $\omega_{2T,-}(K)$. The lower band edge of the two-fermion continuum is denoted by $\omega_{2F,-}(K)$ which strongly overlaps with the two-triplon continuum. The upper fermionic continuum edge lies too high in energy so that it does not appear in Fig. 7. We have also shown the lower band edge $\omega_{1F1T,-}(K)$ and the upper band edge $\omega_{1F1T,+}(K)$ of the fermion-triplon continuum.

The triplon dispersion is maximum at $K = \pi$ and lies energetically always lower than the two-triplon continuum and the two-fermion continuum so that no decay occurs. The fermion dispersion takes its minimum at momentum $K = \pi$ lying below the fermion-triplon continuum. The fermion dispersion almost coincides with the lower band edge of the fermion-triplon continuum for the total momenta $K < 0.8\pi$. This will induce singularities in the spectral densities at the lower band edge of the fermion-triplon continuum.

The contributions of the charge excitations to the low-energy spectrum in Fig. 7 show that the low-energy physics of the SDI phase is indeed very difficult, if not impossible, to describe by a purely magnetic effective Hamiltonian. The approach using elementary fermionic quasiparticles (electrons and holes) works fine in the BI, but it is not appropriate to explain the energy spectrum of the SDI shown in Fig. 7. In terms of elementary fermionic quasiparticles the triplon is an $S = 1$ exciton. One can see from Fig. 7 that this exciton mode has a particularly large binding energy. It is given by the energy difference between the triplon dispersion and the lower band edge of the two-fermion continuum $\omega_{2F,-}(K)$. This large binding energy is evidence of a significant attractive electron-hole interaction in the $S = 1$ channel.

In addition, there are also parts of the two-triplon continuum in Fig. 7 which lie below the two-fermion contin-

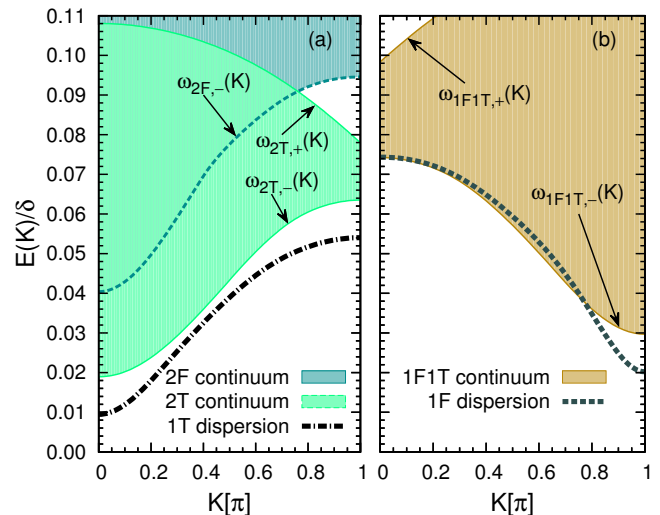


Figure 7. (Color online) The low-energy spectrum of the Hamiltonian (7) for $t = 0.05\delta$ and $U = 1.08\delta$ in the SDI phase. The order of the calculation for the fermion (1F) dispersion is 12 and for the triplon (1T) dispersion it is 10. The two-fermion (2F) continuum, the two-triplon (2T) continuum, and the fermion-triplon (1F1T) continuum are shown as shaded (colored) region. The lower band edge $\omega_{2T,-}(K)$ and the upper band edge $\omega_{2T,+}(K)$ of the two-triplon continuum and the lower band edge $\omega_{2F,-}(K)$ of the two-fermion continuum are shown as well as the lower band edge $\omega_{1F1T,-}(K)$ and the upper band edge $\omega_{1F1T,+}(K)$ of the fermion-triplon continuum. The left panel depicts the excitation spectrum with an even number of fermions and the right panel depicts the excitation spectrum with an odd number of fermions.

uum. This means that even scattering states of two $S = 1$ excitons lie below the scattering states of two elementary fermionic excitations. All these observations underline the difficulty to describe the SDI phase in terms of electrons and holes as elementary excitations of the IHM. Thus the description of the SDI from the dimer limit appears to be suitable.

C. Mott Insulator Phase

The low-lying magnetic excitation spectrum of the gapless MI phase in 1D is described in terms of spin-1/2 quasiparticles called spinons⁴⁴. But starting from a model with some dimerization the natural candidates for the elementary excitations are triplons⁹. For instance, the dispersions, but also dynamic structure factors, approach the ones of uniform chains in the limit of vanishing dimerization. Hence, we proceed with the deepCUT approach to the MI starting from the dimer limit

Fig. 5 shows that the energy difference between the charge gap and the spin gap increases upon increasing Hubbard interaction beyond the first transition at U_{c1} . Clearly, for large values of U the charge fluctuations are very high in energy and the triplon fluctuations determine the low-energy physics of the system. Therefore, it

is a justified first step to derive an effective magnetic low-energy Hamiltonian in terms of triplon operators. For this purpose, the generator $\eta_{f:0;s:0}(\ell)$ is used to separate the sector without any fermions or singlons from the sectors which contain a finite number of fermions and singlons. One should notice that the sector without singlons and fermions still includes triplon fluctuations. The generator $\eta_{f:0;s:0}(\ell)$ is given by

$$\eta_{f:0;s:0}(\ell) := \sum_{j,k} \left(H_{0,0}^{j,k}(\ell) - H_{j,k}^{0,0}(\ell) \right), \quad (22)$$

where $H_{0,0}^{j,k}(\ell)$ stands for the part of the Hamiltonian which annihilates zero number of fermions and singlons and creates j fermions and k singlons. A possible change in the number of triplons is not considered. The application of the generator (22) to the initial Hamiltonian (13) yields an effective Hamiltonian whose magnetic low-energy part is decoupled from the high-energy charge sectors. The low-energy physics of the IHM is determined by this effective Hamiltonian expressed only in terms of triplon operators. We stress that we do not require that this effective Hamiltonian conserves the number of triplons.

In order to check the convergence of the flow equations for the generator (22), the residual off-diagonality (ROD) is plotted in Fig. 8 versus the flow parameter ℓ for various values of the Hubbard interaction U . The residual off-diagonality measures the size of the generator: A large ROD means that the generator is large and vice versa. The rapid vanishing of the ROD upon increasing ℓ signals a good convergence of the CUT. For further details we refer the reader to Ref. 42.

The hopping parameter in Fig. 8 is fixed to 0.05δ . The order in λ of the calculations is 10 and we targeted all the monomials composed of triplon operators only. Fig. 8 shows that the convergence of the flow equations accelerates, i.e., improves, for larger Hubbard interactions. We attribute this behavior to the larger energy separation between the subspace without singlon and fermion excitations and the subspace with a finite number of singlons and fermions. We expect the effective triplon Hamiltonian to be accurate for $U \geq 1.15\delta$ where a convergence of ROD is observed. The transition from the SDI to the MI phase is predicted by DMRG to take place at $U_{c2} \approx 1.085\delta$ ¹⁷. Therefore, it appears that the low-energy triplon Hamiltonian has difficulties to describe the system close to the MI-to-SDI transition. But it should provide a reliable description inside the MI phase.

All the monomials in the low-energy triplon Hamiltonian are of even order in the perturbative parameter λt . Up to order two, they are listed in Table II. The lattice extension of each monomial, i.e., the difference of the index of the rightmost to the leftmost dimer, is equal or less than half of its minimal order. This means that all monomials with minimal order 2 can at most act on two adjacent dimers. This feature helps us to use the same simplification rules as implemented in Ref. 30 in the sub-

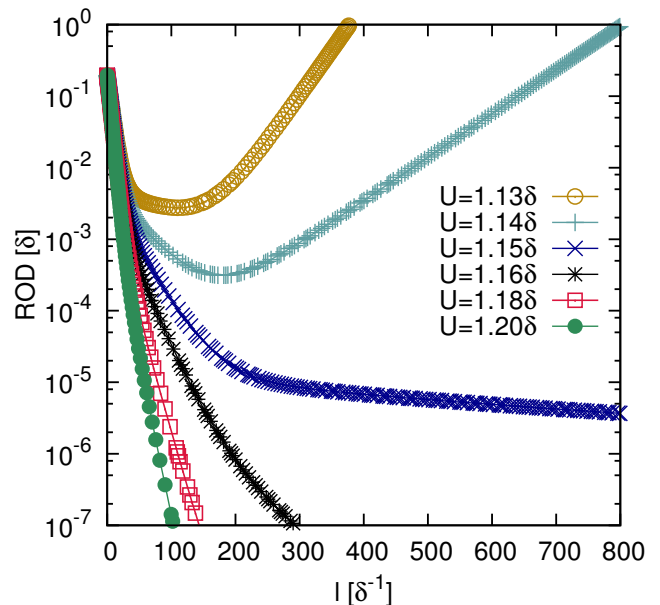


Figure 8. (Color online) The residual off-diagonality (ROD) for the generator $\eta_{f:0;s:0}$ as function of the flow parameter ℓ for various values of U . The hopping parameter is fixed to $t = 0.05\delta$. The order of the calculations is 10 targeting all the monomials composed of triplon operators only.

sequent, second deepCUT applied to analyse the effective triplon Hamiltonian. Henceforth, we switch the formal expansion parameter from λ to $\mu = \lambda^2$ and present all the results based on orders of μ .

The effective triplon Hamiltonian is mapped by a second application of the deepCUT to a final effective Hamiltonian whose ground state and one-triplon sector are separated from higher triplon sectors. This deepCUT allows us to determine the triplon dispersion $\omega_t(K)$. The minimum of the triplon dispersion occurs at the total momentum $K = 0$ so that the spin (triplon) gap is given by $\Delta_s = \omega_t(0)$. Note that one needs to deal with triplon operators only. This enables us to reach much higher orders compared to the case where all the dimer operators (11) matter. Recall that higher orders automatically imply that processes of longer range are tracked. We have been able to reach order 12 in the expansion parameter μ equivalent to order 24 in λ . This maximum order is much higher than the order reached in the computation of the spin gap in Fig. 5.

In the left panel of Fig. 9, the spin gap Δ_s is plotted versus the inverse order in μ for various values of the Hubbard interaction U . The hopping parameter is fixed to $t = 0.05\delta$. The finite order results are extrapolated to infinite order by a linear fit. The extrapolated spin gap is lower than $10^{-4}\delta$ indicating the stabilization of the gapless MI phase for $U \geq 1.15$. The convergence of the results becomes faster as we increase the Hubbard interaction going away from the MI-to-SDI transition point.

We emphasize the importance of the accuracy of the first application of the deepCUT in the derivation of the

Table II. All monomials appearing in the effective triplon Hamiltonian up to minimal order 2 in the relative interdimer hopping λ . The index j runs over dimers and the quantum number m takes the values ± 1 with $\bar{m} = -m$.

#	Monomial	Order
0	$\sum_j \mathbb{1}$	0
1	$\sum_j t_{j,0}^\dagger t_{j,0}$	0
2	$\sum_{j,m} t_{j,m}^\dagger t_{j,m}$	0
3	$\sum_j (t_{j,0}^\dagger t_{j+1,0} + \text{H.c.})$	2
4	$\sum_{j,m} (t_{j,m}^\dagger t_{j+1,m} + \text{H.c.})$	2
5	$\sum_j (t_{j,0}^\dagger t_{j+1,0}^\dagger + \text{H.c.})$	2
6	$\sum_{j,m} (t_{j,m}^\dagger t_{j+1,\bar{m}}^\dagger + \text{H.c.})$	2
7	$\sum_{j,m} (t_{j,m}^\dagger t_{j+1,m}^\dagger t_{j+1,0} - t_{j+1,m} t_{j,m}^\dagger t_{j,0} + \text{H.c.})$	2
8	$\sum_{j,m} (t_{j,0} t_{j+1,m}^\dagger t_{j+1,m} - t_{j+1,0} t_{j,m}^\dagger t_{j,m} + \text{H.c.})$	2
9	$\sum_{j,m} (t_{j,m} t_{j+1,0}^\dagger t_{j+1,\bar{m}} - t_{j+1,m} t_{j,0}^\dagger t_{j,\bar{m}} + \text{H.c.})$	2
10	$\sum_{j,m} t_{j,m}^\dagger t_{j,m} t_{j+1,m}^\dagger t_{j+1,m}$	2
11	$\sum_j t_{j,0}^\dagger t_{j,0} t_{j+1,0}^\dagger t_{j+1,0}$	2
12	$\sum_{j,m} t_{j,m}^\dagger t_{j,m} t_{j+1,\bar{m}}^\dagger t_{j+1,\bar{m}}$	2
13	$\sum_{j,m} (t_{j,m}^\dagger t_{j,0} t_{j+1,\bar{m}}^\dagger t_{j+1,0} + \text{H.c.})$	2
14	$\sum_{j,m} (t_{j,m}^\dagger t_{j,0} t_{j+1,0}^\dagger t_{j+1,m} + \text{H.c.})$	2
15	$\sum_{j,m} (t_{j,m}^\dagger t_{j,m} t_{j+1,0}^\dagger t_{j+1,0} + t_{j+1,m}^\dagger t_{j+1,m} t_{j,0}^\dagger t_{j,0})$	2

low-energy triplon Hamiltonian. In this first step, we target a large number of monomials and a small error may spoil the results obtained in the second step. For example, by reducing the order of calculations in the first step from 10 to 8 we find a slightly negative value for the extrapolated spin gap at $U = 1.15$.

The triplon dispersion $\omega_t(K)$ for various fixed values of the total momentum K is plotted versus the inverse order in the right panel of Fig. 9. The total momenta are chosen close to $K = 0$ where the largest deviation between the results of different orders occurs. The Hubbard interaction U is fixed to 1.15δ and the hopping parameter t is 0.05δ . Again a linear fit is performed to extrapolate the triplon dispersion to infinite order. This extrapolation leads to a numerically gapless triplon dispersion with a linear behavior $\omega_t(K) \propto |K|$ in the vicinity of $K = 0$.

The resulting triplon dispersion is depicted in Fig. 10. The hopping parameter is again $t = 0.05\delta$. The Hubbard interaction in the left panel and in the right panel is set to $U = 1.15\delta$ and $U = 1.20\delta$, respectively. In each panel, various finite order results plus the extrapolated result are shown for comparison. The triplon dispersions at

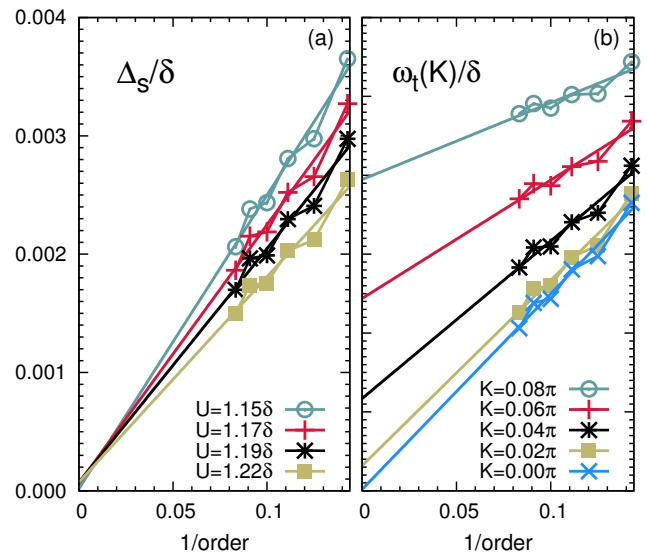


Figure 9. (Color online) Left panel: Spin gap Δ_s versus the inverse order for various U . Right panel: The triplon dispersion $\omega_t(K)$ for various fixed total momentum K versus the inverse order for $U = 1.15\delta$. In both panels the hopping parameter is set to $t = 0.05\delta$. The finite order results are extrapolated to infinite order by a linear fit.

high orders agree well with one another except near the total momenta $K = 0$ and $K = 2\pi$. For these two values of total momentum, the finite order results always lead to a finite spin gap while the extrapolated result yields a numerically gapless excitation.

Such a gapless dispersion with linear behavior around $K = 0$ and $K = 2\pi$ is what one expects in a MI phase. It is interesting to consider the change in the bandwidth of the triplon dispersion in Fig. 10. As the Hubbard interaction decreases from $U = 1.20\delta$ (right panel) to $U = 1.15\delta$ (left panel), the bandwidth of the triplon dispersion increases. Qualitatively, this finding can be understood easily by observing that the magnetic exchange coupling J is $\propto t^2/(U - \delta)$ in leading order in t in the IHM. Thus the generic magnetic energy scale decreases upon increasing U .

We also analyzed the two-triplon sector of the low-energy triplon Hamiltonian searching for possible bound states. It turned out not to be possible to decouple the two-triplon sector completely from the remaining Hilbert space due to divergencies of the flow equations. Thus we proceeded by decoupling the one-triplon sector and taking the remaining off-diagonal interactions between the two-triplon sector and the three-triplon sector into account by an exact diagonalization within the Hilbert space made of up to three triplons⁴². The calculations in finite order find a weakly bound $S = 0$ state. But this singlet bound state lies inside the two-triplon continuum as it can be constructed from the *extrapolated* triplon dispersion. Thus we conclude that it does not exist as a properly bound state, well-separated from the two-triplon continuum. Rather we claim that some sort

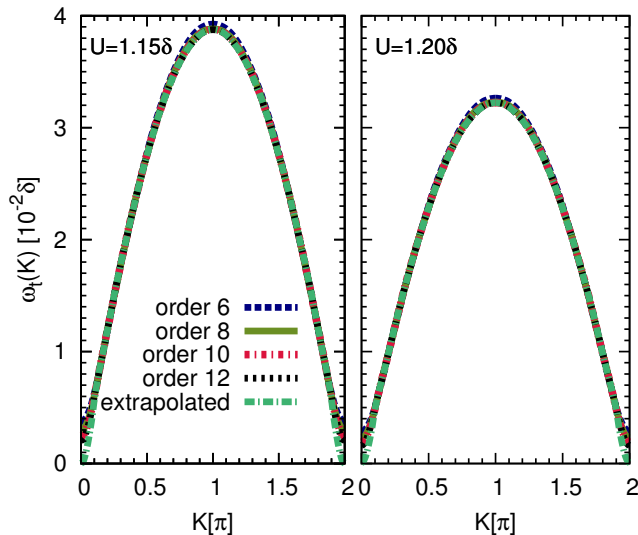


Figure 10. (Color online) Triplon dispersion $\omega_t(K)$ plotted versus the total momentum K in the whole Brillouin zone. The hopping parameter is $t = 0.05\delta$. In the left panel the Hubbard interaction takes the value $U = 1.15\delta$ and in the right panel it is $U = 1.20\delta$. The largest deviations between various orders occur at $K = 0$ and at $K = 2\pi$. A numerically gapless triplon dispersion is obtained by extrapolating the finite order results to infinite order by a linear fit in the inverse order, see right panel in Fig. 9.

of singular resonance exists at the lower boundary of the two-triplon continuum. We presume that it is a divergent power-law as it is found in the sine-Gordon model at particular values of the interaction⁴⁵.

The vanishing of the spin gap and the stabilization of the MI phase in the 1D IHM has been discussed before on the basis of quantum Monte Carlo results⁴⁶ and DMRG results^{15,47} without clear-cut conclusion. Although the position of the second transition point U_{c2} between the SDI and the MI is not determined accurately in our investigation, our results provide clear evidence that the MI phase is stable in the large- U limit. In addition, we obtained quantitative results for the magnetic dispersion of the IHM in the MI phase. Our data support the expectation that the dimer limit can be used as a suitable starting point in CUT-based methods such as deepCUT³⁰, perturbative CUT⁷, and graph-based CUT⁴⁰ to analyze the gapless MI phase in one dimension.

VI. CONCLUSIONS

Strongly correlated systems often give rise to interesting exotic phases which display unconventional excitations. One strategy to find such phases is to study systems with a control parameter which switches from one conventional phase in one limit to another phase in another limit. In the vicinity of the phase transition from one conventional phase to the other the main driving forces counterbalance each other and unexpected mech-

anisms may prevail.

In the present work, we study the ionic Hubbard model (IHM) at half filling where a strong alternation δ from site to site favors the band insulator (BI) phase while a strong on-site repulsion U favors the Mott insulator (MI) phase. Thus, the ratio $g := U/\delta$ is the control parameter in this case. In one dimension, it is established that the BI does not become a MI directly upon increasing g , but an intermediate spontaneously dimerized insulating (SDI) phase appears. The goal of the present paper was to describe the elementary excitations and their dominant interactions in all these three phases using continuous unitary transformations (CUT). This includes the full dependence on the momentum in contrast to many purely numerical approaches. In previous work, this had been achieved in the BI phase only^{18,31,32} starting from fermionic quasiparticles.

In order to be able to describe all three phases in one dimension on equal footing, we chose to start from the dimer limit. This means that we introduce an external dimerization with a comparably weaker interdimer hopping λt where $0 \leq \lambda \leq 1$. Thus, the dimensionless parameter λ is used to truncate the proliferating number of terms in the CUTs. The precise scheme how this is done is the deepCUT introduced earlier³⁰. The dimer limit is obviously advantageous in the description of the spontaneously dimerized phase. But the Mott insulating phase is also known to be describable from the dimer limit because external dimerization is a relevant perturbation⁹. Last, but not least, the fermionic elementary quasiparticles of the BI can also be captured.

Indeed, we could show that the previous results for the fermionic dispersions and the $S = 0$ and $S = 1$ excitons in the BI phase are retrieved from the dimer limit. The dispersions of the fermionic quasiparticles and of the magnetic $S = 1$ triplons agree well with the previous findings. The softening of the $S = 0$ exciton is qualitatively reproduced, but the quantitative agreement is not as good. This is due to the fact that only order 6 could be reached before overlapping continua spoil the convergence of the flow equations. The critical interaction U_{c1} where the BI phase switches to the SDI phase could be determined nicely by the intersection of the ground state energies of a deepCUT starting from the BI limit and from the dimer limit.

In the SDI phase, we could also analyze the dispersions of charge and spin excitations. We found that it is particularly challenging to sort out these excitations in the SDI phase because they all have similar energies. Thus charge and spin degrees of freedom are closely intertwined. This renders a quantitative description difficult, in particular upon approaching the transitions at U_{c1} to the BI phase and at U_{c2} to the MI phase. The value of U_{c2} can only be estimated roughly because the finite spin gap, induced by the spontaneous dimerization in the SDI phase, vanishes only very weakly, i.e., exponentially, upon $U \rightarrow U_{c2}$ since this transition is of Kosterlitz-Thouless type¹³.

For the magnetic excitations in the MI, we used the

deepCUT in two steps. First, we systematically derived an effective Hamiltonian in terms of triplons, i.e., magnetic $S = 1$ quasiparticles. In this step, the charge degrees of freedom are disentangled from the magnetic ones. In a subsequent, second deepCUT the magnetic effective Hamiltonian is unitarily transformed such that the number of triplons becomes a conserved quantity. This allows one to read off the magnetic dispersion directly, for example its minimum defining the spin gap. The extrapolation of the spin gap to infinite order in $\mu = \lambda^2$ reveals that the MI is a phase with massless magnetic excitations.

We summarize that our study yields results for the full momentum dependence of the charge and spin excitations in all three phases in one dimension. These results are obtained on equal footing by introducing an auxiliary dimerization which is sent to zero finally. The approach is based on a real space representation of the deepCUT. Since such an approach only captures processes up to a certain range, here up to 24 lattice spacings, the immediate vicinities of the phase transitions cannot be described quantitatively. Future work is called for to improve on this point.

We emphasize that the approach based on the concept of the deepCUT has the advantage to be generalizable to higher dimensions. We recall that the nature of the intermediate phase in two dimensions is still highly controversial^{19–23}. Surely, the band insulator limit can be used to look for the nature of the modes which become soft upon increasing interaction, indicating the instability of the BI. In the Mott insulating phase, the starting point of a long-range ordered magnet suggests itself. A dimerized limit is conceivable, but so far no evidence is known to us that this is an ordering pattern likely to form the intermediate phase in more than one dimension.

ACKNOWLEDGMENT

We would like to thank Kai P. Schmidt for fruitful discussions. We gratefully acknowledge financial support by the NRW-Forschungsschule “Forschung mit Synchrotronstrahlung in den Nano- und Biowissenschaften”, the Mercator Research Center Ruhr “Elementary excitations and their non-equilibrium dynamics in novel materials: From Mott insulators to unconventional superconductors”, and the Helmholtz Virtual-Institute “New states of matter and their excitations”.

Appendix A: Simplification Rules

In this section, we discuss the simplification rules (SRs) that we employed in the dimer limit analysis of the IHM (13). When we are interested only in some coefficients of the effective Hamiltonian, only a small part of the other coefficients is relevant as intermediate result. Mathematically, the relevance of a monomial can be characterized by its *maximal order*³⁰. The SRs allow

us to estimate this maximal order and to discard irrelevant monomials and contributions early in the calculation, reducing both runtime and memory consumption drastically. The concept of SRs and the precise definition of the maximal order are introduced in Ref. 30 and the reader is referred to this reference for details.

We distinguish *a priori* and *a posteriori* SRs: The *a posteriori* SRs are applied to the individual monomials that occur by evaluating the commutator of the flow equation (14), while the *a priori* SRs are used to estimate the maximal order based directly on the arguments that enter the commutator without evaluating it explicitly. In general, the *a posteriori* SRs eliminate superfluous contributions more thoroughly than their *a priori* counterparts, but the *a priori* SRs can prevent the cumbersome evaluation of the commutator at all when none of the resulting monomials are relevant. So for the best computational performance, the combined application of both versions of SRs is preferred.

We classify the dimer excitation operators (11) into a boson and a fermion group. The boson group contains the singlon (11c) and the three triplon operators (11b). The fermion group includes the four fermion operators (11a) which act on the left site $f_l^{(\dagger)}$ and on the right site $f_r^{(\dagger)}$ of a dimer with two possible spin quantum numbers. According to the internal site that a fermion operator acts we define two types of fermion operators: ‘left’ and ‘right’. The off-diagonal elements in the Hamiltonian (13) describe various kinds of annihilation and creation processes between and among fermions and bosons. This makes it difficult to find efficient and flexible SRs especially if sectors with finite numbers of fermions and/or bosons are targeted.

In the following, two kinds of SRs are introduced. The first one are the basic SRs which are not very efficient, but flexible. Both, an *a posteriori* and an *a priori* version exist. They can be applied if sectors with a specific number of bosons and fermions are targeted. In the basic SRs, only the number of creation and annihilation operators of each monomial is considered.

In the second kind of SRs, called extended SRs, the lattice structure of the monomials is also taken into account. Here, we derive an *a posteriori* version only. The extended SR works efficiently for the ground state and to some extent for the one-fermion sector. It is also used for the derivation of the low-energy triplon Hamiltonian where all the triplon operators are targeted. But the present extended SR needs to be generalized if higher fermion sectors or sectors with a mixed number of bosons and fermions are targeted.

Before describing the basic and the extended SRs, let us consider the general structure of off-diagonal terms in the Hamiltonian (13). We emphasize that the first order generator terms are sufficient to consider for deriving the SRs although higher order terms with more complex structures also appear during the flow³⁰. On the one hand, the more complex structure allows for more complicated cancellations. On the other hand, the higher or-

der limits the possible effect for given targeted order. In other words, the more complex term can be understood as being built by iterated multiplication or commutation with the first order generator term.

Among the first order generator terms, only the three structures following are important to determine the maximal orders

$$\eta^{(a)} \propto \sum_j f_{j;l}^\dagger f_{j+1;r}^\dagger + \text{H.c.}, \quad (\text{A1a})$$

$$\eta^{(b)} \propto \sum_j b_j^\dagger f_{j;p} f_{j+1;p}^\dagger + \text{H.c.} \quad ; \quad p = l, r, \quad (\text{A1b})$$

$$\eta^{(c)} \propto \sum_j b_j^\dagger b_{j+1}^\dagger f_{j;l} f_{j+1;r} + \text{H.c.}, \quad (\text{A1c})$$

where the boson operator b^\dagger stands either for a singlon or for a triplon operator and we omitted the spin index of the fermion operators to lighten the notation and because they play no role in the following considerations.

1. The Basic Simplification Rules

We start our derivation with the basic *a posteriori* simplification rule. In the first step, we focus on the number of annihilation and creation operators which can be canceled by commutation with the generator structures (A1). The first term $\eta^{(a)}$ can cancel two fermion creation or annihilation operators only if they act on *different* intradimer positions which are either the left $p = l$ or the right site $p = r$. In other words, the generator $\eta^{(a)}$ can only cancel two fermion operators of different types. This reflects the conservation of the total charge of the system. Two creation or annihilation operators of the same type need at least two commutations with the generator $\eta^{(a)}$ to be canceled. This property allows us to make the SRs dependent on the fermion type using the same strategy as in Ref. 18. The net effect of the second term $\eta^{(b)}$ is to cancel one boson operator. The third term $\eta^{(c)}$ transforms two boson operators into two fermion operators of different types.

We aim at finding an upper bound for the maximal order of a monomial A if sectors with up to q_b bosons and up to q_f fermions are targeted up to order n . We focus on the creation operators supposing that the monomial A creates c_b boson and c_f fermions. The annihilation operators can be treated in the same way. At first, we discuss the situation where no fermions are targeted, but q_b bosons. Then we aim at keeping q_f fermion operators of the monomial A such that the maximal order is overestimated. The number of boson operators which have to be canceled reads as

$$c'_b := \max(c_b - q_b, 0). \quad (\text{A2})$$

If c'_b is even, we transform all these boson operators to fermion operators using $\eta^{(c)}$. If c'_b is odd, the even number $c'_b - 1$ of boson operators are transformed into fermion

operators and the remaining boson operator is canceled by $\eta^{(b)}$. This procedure requires $\left\lceil \frac{c'_b}{2} \right\rceil$ commutations and produces $2 \left\lfloor \frac{c'_b}{2} \right\rfloor$ additional fermion operators. We use the ceiling brackets $\lceil \cdot \rceil$ for the smallest integer larger or equal to the argument while the flooring brackets $\lfloor \cdot \rfloor$ stand for the largest integer smaller or equal to the argument in the brackets. Half of these additional fermion operators are of the type f_l and the other half are of type f_r . Therefore, the total number of fermion operators of type ‘left’ and ‘right’ which have to be canceled is given by

$$c'_{f_l} = c_{f_l} + \left\lceil \frac{c'_b}{2} \right\rceil, \quad (\text{A3a})$$

$$c'_{f_r} = c_{f_r} + \left\lfloor \frac{c'_b}{2} \right\rfloor, \quad (\text{A3b})$$

where c_{f_l} and c_{f_r} are the initial numbers of fermion operators of type ‘left’ and ‘right’ in the monomial A .

The fermion operators can be canceled by commutations with the term $\eta^{(a)}$. This term always cancels two fermions of different types, i.e., on different intradimer positions. Fermion operators of the same type need one commutation each. Hence, the number of commutations necessary to eliminate all the boson (A2) and the fermion (A3) operators is given by

$$K_{0,q_b}^c = \left\lceil \frac{c'_b}{2} \right\rceil + \max(c'_{f_l}, c'_{f_r}). \quad (\text{A4})$$

This equation can be generalized to K_{q_f,q_b}^c if sectors with up to q_b bosons and q_f fermions are targeted. In this case, one needs to keep q_f fermion operators of monomial A such that the number of commutations K_{q_f,q_b}^c is minimized.

We divide the fermion operators into pairs. Each pair contains one ‘left’ and one ‘right’ operator. First, we keep the fermion operators which do not form pairs. In this way, one can save one commutation for each fermion operator. The remaining fermion operators are all in pairs. This saves one commutation for each pair of operators. In this way, we obtain

$$K_{q_f,q_b}^c = K_{0,q_b}^c - d_1^c - \left\lfloor \frac{d_2^c}{2} \right\rfloor, \quad (\text{A5})$$

where d_1^c and d_2^c are defined as

$$d_1^c := \min(q_f, |c'_{f_l} - c'_{f_r}|), \quad (\text{A6a})$$

$$d_2^c := \min(q_f - d_1^c, c'_{f_l} + c'_{f_r} - d_1^c). \quad (\text{A6b})$$

The annihilation part of monomial A can be analyzed in the same way and leads to K_{q_f,q_b}^a . Finally, the upper bound for the maximal order of the monomial A is given by³⁰

$$\tilde{O}_{\max}(A) = n - K_{q_f,q_b}^c - K_{q_f,q_b}^a, \quad (\text{A7})$$

where n is the order of calculations. The monomial A has no effect on the targeted quantities up to order n and can be neglected if

$$\tilde{O}_{\max}(A) < O_{\min}(A). \quad (\text{A8})$$

We refer to this analysis as the basic *a posteriori* SR.

Now, we explain the basic *a priori* SR for the commutator $[T, D] = TD - DT$. We focus on the product TD . The product DT can be treated in the same way. All we need to do is to bound the number of creation and annihilation operators which remain after normal-ordering from below.

Suppose c_T^i and a_T^i are the numbers of creation and annihilation operators of type i , respectively, in the monomial T . The index i refers to the eight possible operators (singlon, triplons, and fermions) that can appear on a dimer, cf. Tab. I. Similarly, there are c_D^i creation operators and a_D^i annihilation operators of type i in the monomial D . Only operators of the same type can cancel each other in the process of normal-ordering. Therefore, the number of creation and annihilation operators of type i of the product TD can be bounded from below by

$$c_{TD}^i \geq \tilde{c}_{TD}^i := c_T^i + c_D^i - s_{TD}^i, \quad (\text{A9a})$$

$$a_{TD}^i \geq \tilde{a}_{TD}^i := a_D^i + a_T^i - s_{TD}^i, \quad (\text{A9b})$$

where $s_{TD}^i := \min(a_T^i, c_D^i)$. Subsequently, for the number of boson operators and the number of ‘left’ and ‘right’ fermion operators we find

$$c_{TD}^b \geq \tilde{c}_{TD}^b := \sum_{i \in b} \tilde{c}_{TD}^i, \quad (\text{A10a})$$

$$c_{TD}^{f_r} \geq \tilde{c}_{TD}^{f_r} := \sum_{i \in f_r} \tilde{c}_{TD}^i, \quad (\text{A10b})$$

$$c_{TD}^{f_l} \geq \tilde{c}_{TD}^{f_l} := \sum_{i \in f_l} \tilde{c}_{TD}^i, \quad (\text{A10c})$$

where b stands for bosons and f_l and f_r stand for ‘left’ and ‘right’ fermions. Analogous relations as (A10) are valid for the annihilation operators in TD .

On the basis of the numbers c_{TD}^b , $c_{TD}^{f_r}$, $c_{TD}^{f_l}$, a_{TD}^b , $a_{TD}^{f_r}$, and $a_{TD}^{f_l}$, we can estimate the maximal order of the product TD using the relation (A7). Finally, the commutator $[T, D]$ has no effect on the targeted quantities up to order n and can be ignored if

$$\max\left(\tilde{O}_{\max}(TD), \tilde{O}_{\max}(DT)\right) < O_{\min}(T) + O_{\min}(D). \quad (\text{A11})$$

This basic *a priori* SR can be used in addition to the basic *a posteriori* SR (A8) or in addition to the extended *a posteriori* SR that is presented in the next subsection, in order to increase the speed of the deepCUT algorithm.

2. The Extended A Posteriori Simplification Rule

The upper bound (A7) for the maximal order of the monomial A can be lowered by taking into account the

lattice structure of the generator terms (A1). The first term $\eta^{(a)}$ cancels two fermions of different type, but only on nearest-neighbor (n.n.) dimers. The third term $\eta^{(c)}$ transforms two n.n. bosons into two n.n. fermions of different type. Special attention has to be paid to the second term $\eta^{(b)}$. This term can cancel one boson accompanied with a n.n. hopping process for a fermion. This additional hopping process makes it difficult to derive an efficient extended SR as done in Refs. 18 and 30. In the following, we derive a lower bound for the number of commutations required to cancel all the fermion and boson creation operators of monomial A . The annihilation part of monomial A can be treated in the same way.

Similar to Ref. 30, we consider the monomial A and split the cluster of sites on which creation operators act into different *linked* subclusters. We define $K[\mathcal{C}]$ as the number of commutations needed to cancel all operators of the linked subcluster \mathcal{C} . We have to bound this number of commutations from below in order to find an upper bound for the maximal order of monomial A . The size of each linked subcluster can be reduced based on the following inequalities

$$K[\otimes-\oplus-\mathcal{C}'] = K[\otimes-\oplus] + K[\mathcal{C}'] \geq 1 + K[\mathcal{C}'], \quad (\text{A12a})$$

$$K[\bullet-\bullet-\mathcal{C}'] = K[\bullet-\bullet] + K[\mathcal{C}'] \geq 2 + K[\mathcal{C}'], \quad (\text{A12b})$$

$$K[\bullet-\otimes-\mathcal{C}'] = K[\bullet-\otimes] + K[\mathcal{C}'] \geq 2 + K[\mathcal{C}'], \quad (\text{A12c})$$

$$K[\otimes-\bullet-\mathcal{C}'] \geq 1 + K[\otimes-\mathcal{C}'], \quad (\text{A12d})$$

$$K[\otimes-\otimes-\mathcal{C}'] \geq 1 + K[\otimes-\mathcal{C}'], \quad (\text{A12e})$$

where the symbols \otimes and \oplus denote the two possible fermion operators on a dimer, the symbol \bullet stands for a boson operator on a dimer, and \mathcal{C}' stands for the remaining part of the initial subcluster. For instance, on the left hand side of the first equation (A12a) the two n.n. fermion operators of different type $\otimes-\oplus$ are linked to the remaining part \mathcal{C}' . The validity of Eqs. (A12) can be derived on the basis of the structure of the generator terms (A1).

As an example, let us illustrate that one cannot cancel the linked fermion and boson operators $\otimes-\bullet$ in Eq. (A12d). Consider a linked cluster of the form

$$\mathcal{C} = \otimes-\underbrace{\bullet-\bullet-\dots-\bullet-\bullet}_n-\oplus, \quad (\text{A13})$$

where two different fermion operators at the two outer ends of the cluster \mathcal{C} are linked by n boson operators. By n applications of the generator term (A1b), one can cancel all the boson operators and bring the two fermion operators to adjacent dimers. This pair of n.n. fermion operators can also be canceled by one additional commutation with the generator term (A1a). Hence, the total number of commutations required to cancel the cluster (A13) is $n + 1$.

The scheme in Eqs. (A12) reduces a linked subcluster of operators to at most an individual fermion or boson operator. A single boson operator requires two commutations and a single fermion operator one commutation

to be canceled. In this manner, we can find the minimum number of commutations $\tilde{K}[\mathcal{C}]$ to cancel all operators of the linked subcluster \mathcal{C} . Then, the minimum number of commutations necessary to cancel all the creation operators of monomial A is given by

$$K_{0,0}^c = \sum_{\mathcal{C}} \tilde{K}[\mathcal{C}], \quad (\text{A14})$$

where the sum runs over all linked subcluster of creation operators in the monomial A . Similarly, we can analyze the annihilation operators of the monomial A . Finally, the maximal order is calculated by Eq. (A7). We refer to this analysis as extended *a posteriori* SR. This extended *a posteriori* SR is applied in three different cases that we discuss in the following.

a. The ground state and the one-fermion sector

For the ground state, one can make the scheme presented in Eq. (A12) spin-dependent. This takes into account that the two fermion operators in Eq. (A12a) can be canceled only if they have *different* spin. In this case, we should take care of the spin of the fermion operator in Eq. (A12d). The spin of the fermion operator will be changed from the left to the right hand side in Eq. (A12d) if the boson operator is a triplon with the magnetic number ± 1 .

This spin-dependent extended SR saves a factor of about 8 in the number of representatives compared to

the basic SR if the ground state is targeted. We also used this extended SR to describe the one-fermion sector based on the simple estimate $K_{1,0} = K_{0,0} - 1$ for both the creation and the annihilation operators. This relation can always be used in Eq. (A7) because a fermion operator requires at most one commutation to be canceled. For higher fermion sectors, however, such a simple estimate does not work efficiently and further modifications are required.

b. Derivation of the triplon Hamiltonian

The extended *a posteriori* SR is employed also in the derivation of the effective triplon Hamiltonian in subsection VC. In this deepCUT application, all triplon operators are targeted and we need to cancel the singlon and the fermion operators. The cluster of creation and annihilation operators are made of singlon and fermion operators only, ignoring the triplon operators. In this case, the extended SR can not be made spin-dependent, as in the ground state case, because two fermions with the same spin can be transformed into a triplon operator by one commutation.

The number of representatives which remain when applying this extended SR differs by a factor of about 2 from the real number of representatives which we need to describe the triplon Hamiltonian up to order 10. This indicates that the extended SR is working incredibly well also for the derivation of the effective triplon Hamiltonian.

* mohsen.hafez@tu-dortmund.de

† nils.drescher@tu-dortmund.de

‡ goetz.uhrig@tu-dortmund.de

¹ F. Gebhard, *The Mott Metal-Insulator Transition* (Springer, Berlin, 1997).

² M. Imada, A. Fujimori, and Y. Tokura, *Rev. Mod. Phys.* **70**, 1039 (1998).

³ J. des Cloizeaux and J. J. Pearson, *Phys. Rev.* **128**, 2131 (1962).

⁴ L. D. Faddeev and L. A. Takhtajan, *Phys. Lett.* **85A**, 375 (1981).

⁵ M. C. Cross and D. S. Fisher, *Phys. Rev. B* **19**, 402 (1979).

⁶ G. S. Uhrig, F. Schönfeld, M. Laukamp, and E. Dagotto, *Eur. Phys. J. B* **7**, 67 (1999).

⁷ C. Knetter and G. Uhrig, *The European Physical Journal B* **13**, 209 (2000).

⁸ W. Zheng, C. J. Hamer, R. R. P. Singh, S. Trebst, and H. Monien, *Phys. Rev. B* **63**, 144411 (2001).

⁹ K. P. Schmidt and G. S. Uhrig, *Phys. Rev. Lett.* **90**, 227204 (2003).

¹⁰ T. Papenbrock, T. Barnes, D. J. Dean, M. V. Stoitsov, and M. R. Strayer, *Phys. Rev. B* **68**, 024416 (2003).

¹¹ A. Auerbach, *Interacting Electrons and Quantum Magnetism*, Graduate Texts in Contemporary Physics (Springer, New York, 1994).

¹² L. Balents, *Nature* **464**, 199 (2010).

¹³ M. Fabrizio, A. O. Gogolin, and A. A. Nersesyan, *Phys. Rev. Lett.* **83**, 2014 (1999).

¹⁴ M. E. Torio, A. A. Aligia, and H. A. Ceccatto, *Phys. Rev. B* **64**, 121105 (2001).

¹⁵ S. R. Manmana, V. Meden, R. M. Noack, and K. Schönhammer, *Phys. Rev. B* **70**, 155115 (2004).

¹⁶ H. Otsuka and M. Nakamura, *Phys. Rev. B* **71**, 155105 (2005).

¹⁷ L. Tincani, R. M. Noack, and D. Baeriswyl, *Phys. Rev. B* **79**, 165109 (2009).

¹⁸ M. Hafez Torbati, N. A. Drescher, and G. S. Uhrig, *Phys. Rev. B* **89**, 245126 (2014).

¹⁹ A. Garg, H. R. Krishnamurthy, and M. Randeria, *Phys. Rev. Lett.* **97**, 046403 (2006).

²⁰ S. S. Kancharla and E. Dagotto, *Phys. Rev. Lett.* **98**, 016402 (2007).

²¹ N. Paris, K. Bouadim, F. Hébert, G. G. Batrouni, and R. T. Scalettar, *Phys. Rev. Lett.* **98**, 046403 (2007).

²² L. Craco, P. Lombardo, R. Hayn, G. I. Japaridze, and E. Müller-Hartmann, *Phys. Rev. B* **78**, 075121 (2008).

²³ H.-M. Chen, H. Zhao, H.-Q. Lin, and C.-Q. Wu, *New Journal of Physics* **12**, 093021 (2010).

²⁴ P. J. Strebler and Z. G. Soos, *The Journal of Chemical Physics* **53**, 4077 (1970).

- ²⁵ Z. G. Soos and S. Mazumdar, *Phys. Rev. B* **18**, 1991 (1978).
- ²⁶ N. Nagaosa and J. Takimoto, *Journal of the Physical Society of Japan* **55**, 2735 (1986).
- ²⁷ J. B. Torrance, J. E. Vazquez, J. J. Mayerle, and V. Y. Lee, *Phys. Rev. Lett.* **46**, 253 (1981).
- ²⁸ T. Egami, S. Ishihara, and M. Tachiki, *Science* **261**, 1307 (1993).
- ²⁹ K. Kobayashi, S. Horiuchi, R. Kumai, F. Kagawa, Y. Murakami, and Y. Tokura, *Phys. Rev. Lett.* **108**, 237601 (2012).
- ³⁰ H. Krull, N. A. Drescher, and G. S. Uhrig, *Phys. Rev. B* **86**, 125113 (2012).
- ³¹ M. Hafez and S. A. Jafari, *The European Physical Journal B* **78**, 323 (2010).
- ³² M. Hafez and M. R. Abolhassani, *Journal of Physics: Condensed Matter* **23**, 245602 (2011).
- ³³ J. Oitmaa, C. Hamer, and W. Zheng, *Series Expansion Methods for Strongly Interacting Lattice Models* (Cambridge University Press, Cambridge, 2006).
- ³⁴ S. Duffe and G. Uhrig, *The European Physical Journal B* **84**, 475 (2011).
- ³⁵ F. Wegner, *Annalen der Physik* **506**, 77 (1994).
- ³⁶ S. Kehrein, *The Flow Equation Approach to Many-Particle Systems*, Springer Tracts in Modern Physics, Vol. 217 (Springer, Berlin, 2006).
- ³⁷ C. Knetter, K. Schmidt, and G. Uhrig, *The European Physical Journal B* **36**, 525 (2003).
- ³⁸ H.-Y. Yang, A. M. Läuchli, F. Mila, and K. P. Schmidt, *Phys. Rev. Lett.* **105**, 267204 (2010).
- ³⁹ S. Dusuel and G. S. Uhrig, *Journal of Physics A: Mathematical and General* **37**, 9275 (2004).
- ⁴⁰ H. Y. Yang and K. P. Schmidt, *EPL (Europhysics Letters)* **94**, 17004 (2011).
- ⁴¹ B. Fauseweh and G. S. Uhrig, *Phys. Rev. B* **87**, 184406 (2013).
- ⁴² T. Fischer, S. Duffe, and G. S. Uhrig, *New Journal of Physics* **12**, 033048 (2010).
- ⁴³ G. Müller, H. Thomas, H. Beck, and J. C. Bonner, *Phys. Rev. B* **24**, 1429 (1981).
- ⁴⁴ M. Karbach, G. Müller, A. H. Bougourzi, A. Fledderjohann, and K.-H. Mütter, *Phys. Rev. B* **55**, 12510 (1997).
- ⁴⁵ A. O. Gogolin, A. A. Nersesyan, and A. M. Tsvelik, *Bosonization and Strongly Correlated Systems* (Cambridge University Press, Cambridge, 1998).
- ⁴⁶ T. Wilkens and R. M. Martin, *Phys. Rev. B* **63**, 235108 (2001).
- ⁴⁷ A. P. Kampf, M. Sekania, G. I. Japaridze, and P. Brune, *Journal of Physics: Condensed Matter* **15**, 5895 (2003).